



Brain-machine interface learning is facilitated by specific patterning of distributed cortical feedback

Aamir Abbasi, Henri Lassagne, Luc Estebanez, Dorian Goueytes, Daniel Shulz, Valerie Ego-Stengel

► To cite this version:

Aamir Abbasi, Henri Lassagne, Luc Estebanez, Dorian Goueytes, Daniel Shulz, et al.. Brain-machine interface learning is facilitated by specific patterning of distributed cortical feedback. *Science Advances*, 2023, 9 (38), pp.eadh1328. 10.1126/sciadv.adh1328 . hal-04220009

HAL Id: hal-04220009

<https://hal.science/hal-04220009>

Submitted on 27 Sep 2023

HAL is a multi-disciplinary open access archive for the deposit and dissemination of scientific research documents, whether they are published or not. The documents may come from teaching and research institutions in France or abroad, or from public or private research centers.

L'archive ouverte pluridisciplinaire **HAL**, est destinée au dépôt et à la diffusion de documents scientifiques de niveau recherche, publiés ou non, émanant des établissements d'enseignement et de recherche français ou étrangers, des laboratoires publics ou privés.



Distributed under a Creative Commons Attribution - NonCommercial 4.0 International License

NEUROSCIENCE

Brain-machine interface learning is facilitated by specific patterning of distributed cortical feedback

Aamir Abbasi[†], Henri Lassagne[†], Luc Estebanez[†], Dorian Goueytes, Daniel E. Shulz[‡], Valerie Ego-Stengel^{‡*}

Neuroprosthetics offer great hope for motor-impaired patients. One obstacle is that fine motor control requires near-instantaneous, rich somatosensory feedback. Such distributed feedback may be recreated in a brain-machine interface using distributed artificial stimulation across the cortical surface. Here, we hypothesized that neuronal stimulation must be contiguous in its spatiotemporal dynamics to be efficiently integrated by sensorimotor circuits. Using a closed-loop brain-machine interface, we trained head-fixed mice to control a virtual cursor by modulating the activity of motor cortex neurons. We provided artificial feedback in real time with distributed optogenetic stimulation patterns in the primary somatosensory cortex. Mice developed a specific motor strategy and succeeded to learn the task only when the optogenetic feedback pattern was spatially and temporally contiguous while it moved across the topography of the somatosensory cortex. These results reveal spatiotemporal properties of the sensorimotor cortical integration that set constraints on the design of neuroprosthetics.

INTRODUCTION

Accurate limb control requires somatosensory feedback. For instance, local peripheral anesthesia blocking afferent tactile sensation in humans reduces dexterity and impairs fine motor control of the hand (1, 2). Similarly, cortical inactivation of somatosensory cortex in animals has profound effects on motor control (3, 4). The critical role of somatosensory feedback has also been described in studies of patients that suffer from severe tactile or proprioceptive deficits. These patients learn to rely extensively on visual feedback, but remain unable to manage normal motor control (5–7).

In the context of neuroprosthetics, proprioceptive and touch-like feedback originating from the prosthesis improves control (8) and enables texture-like percepts that cannot be obtained through visual feedback alone (9). Such artificial touch-like information has been provided through direct activation of the cerebral cortex via electrical stimulation (8, 10–14) or optogenetics (15, 16). Beyond the choice of the neuronal stimulation technology, an important challenge is the design of the geometry and dynamics of the feedback patterns used to provide relevant sensory feedback information.

The design of artificial sensory feedback is particularly critical for replicating the functionality of a spatially distributed sense such as touch (17). Temporal modulation of one single stimulation channel, such as realized by optogenetic stimulation of the primary somatosensory cortex (S1) in the brain-machine interface experiments of Prsa *et al.* (16), cannot suffice in this case. Rather, many independent channels of stimulation will be necessary to convey tactile information arising from different peripheral locations. Recent approaches have implemented simultaneous artificial stimulations at multiple locations in the somatosensory cortex (18, 19). However, it remains unclear whether any arbitrary feedback pattern

can be applied or whether the somatosensory-motor cortical areas can only integrate efficiently inputs with a specific type of spatiotemporal structure matched to the classical somatosensory topography (20).

Here, we take advantage of the well-known whisker system of the mouse to explore this question (21, 22). Anatomically, the representation of the mouse snout in S1 is organized into distinct columns, called barrels, that each receive dominant inputs from one corresponding whisker. These inputs combine with dense subcortical and intracortical lateral connectivity (23, 24) and give rise to rich encoding of complex multiwhisker features, which can be found at the level of individual neurons as well as in the cortical map [summarized in (25)]. Specifically, given the strong tuning of S1 neurons to the direction of bar-like multiwhisker deflections on the snout (26, 27), and their tuning to progressive movement of objects across the whiskerpad (28), we hypothesized that stimulations that generate spiking activity in spatiotemporally contiguous barrel cortex locations may be more efficiently integrated by the mice.

We tested this hypothesis by training mice to control a virtual cursor using the modulation of the activity of a few neurons, called Master neurons, recorded in the whisker area of the primary motor cortex (M1) (29). Mice received online one of five different spatiotemporal patterns of cortical feedback generating spiking activity in S1. These patterns ranged from a sweeping, bar-like feedback where the barrels that were simultaneously or sequentially activated were all contiguous, up to a spatiotemporally fully randomized pattern, also including a condition without feedback. The inputs were delivered on the surface of the cortex by photostimulation of subsets of always 5 barrels among the 22 most caudal barrels. We focused on the impact of changes in the structure of patterned stimulation, while the total surface area, intensity, and temporal frequency of stimulation remained always constant. We found that learning was largely dependent on the structure of the feedback and was highest in the bar-like feedback condition, where the photostimulated barrels are spatially and temporally contiguous. Learning in this specific condition revealed voluntary

Copyright © 2023 The Authors, some rights reserved; exclusive licensee American Association for the Advancement of Science. No claim to original U.S. Government Works. Distributed under a Creative Commons Attribution License 4.0 (CC BY).

Université Paris-Saclay, CNRS, Institut des Neurosciences Paris-Saclay (NeuroPSI), 91400 Saclay, France.

*Corresponding author. Email: valerie.ego-stengel@cnr.fr

†These authors contributed equally to this work.

‡These authors contributed equally to this work.

control of the motor cortical activity. In particular, we found that the neuronal activity that drove the virtual cursor became dominated by one of the Master neurons.

RESULTS

Patterned optogenetic feedback on S1 enables learning in a brain-machine interface

We implanted a total of 16 mice with a chronic, closed-loop brain-machine interface consisting of a head fixation bar, chronic silicon tetrodes in layer 5 of whisker M1 (Fig. 1, A and B, and figs. S1 and S2), and a chronic optical window over the S1 area (see Materials and Methods and fig. S8).

After initial sessions where we habituated the mice to remain head-fixed and lick for water, we trained the mice to solve a one-dimensional cursor control task via the brain-machine interface. To this aim, we sorted three “Master” neurons from the raw M1 neuronal activity (seven Master neurons in two mice, see Materials and Methods). The activity of these neurons controlled the movements of a virtual cursor during the sessions. Their summed firing rate was measured every 10 ms and was smoothed with a 100-ms kernel. It was then normalized by the firing rate distribution measured during a 3-min baseline at the start of each session. Last, we discretized the normalized values into eight positions of a virtual cursor (see Materials and Methods, Fig. 1C, and fig. S3).

Whenever the virtual cursor was in the rewardable position (Fig. 1, C to E, only in position 5, except in our first experiments; see

Materials and Methods), the mice could obtain a water droplet by licking a port located next to their tongue. Water rewards could be triggered only by licking on the spout. Therefore, in the absence of licking while the virtual cursor was in the rewardable position, no water was made available to the mouse. During the task, the current position of the virtual cursor was provided online to the mice through patterned optogenetic stimulation of S1 that triggered local, low-latency spiking activity (see Materials and Methods). The mice expressed constitutively channelrhodopsin in pyramidal neurons (*Emx-Cre;Ai27* strain) (30). The photostimulations were dynamically updated, with an intrinsic hardware latency of 12 ± 5 ms from the firing of the Master neurons to the corresponding photostimulation update (15).

At each time point, the pattern of cortical illumination consisted of focused spots that targeted five of the S1 barrels. We arranged these spots to form a bar-like arrangement of barrel activations, sweeping on barrels corresponding to caudal whiskers for position 1 of the virtual cursor, up to rostral whiskers for position 8 (Bar feedback; Fig. 1, D and E).

A 30-min training session per day was delivered during 5 days. To obtain more rewards, the mice had to increase the amount of time during which the virtual cursor was in the rewardable position, and/or improve their ability to lick in those time windows.

When Bar feedback was provided (Fig. 2A, top), the mice were able to increase their performance within the five consecutive training sessions (example in Fig. 2B, top). We measured the performance in terms of both reward frequency (number of rewards,

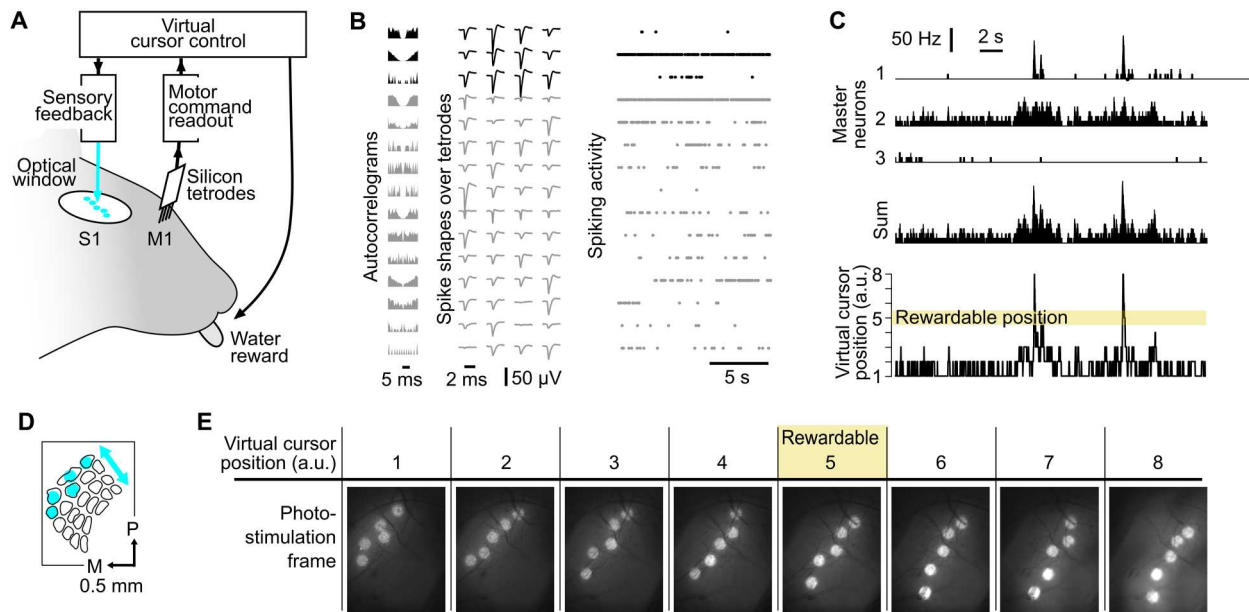


Fig. 1. Mice controlled a virtual cursor using whisker M1 neuronal activity while online optogenetic feedback was delivered to whisker S1. (A) General view of the closed-loop interface. The mice were head-fixed. A chronic silicon probe in M1 readout spiking activity and a chronic optical window over S1 allowed delivery of a photostimulation feedback. (B) Action potentials from 15 single units obtained during baseline activity in M1. The autocorrelograms (left), the spike shapes on the tetrodes (middle), and the spiking activity in time (right) are shown for each single unit. Black, Master neurons that are selected to control the virtual cursor; gray, neighboring neurons recorded simultaneously. (C) Example Master neuron activity and corresponding virtual cursor position. Top, time histograms of the three Master neuron activities; middle, sum of their activity; bottom, position of the virtual cursor computed from the summed activity of the Master neurons. The virtual cursor must be in position 5 for the mouse to obtain a reward by licking. a.u., arbitrary units. Bin size, 10 ms. (D) Schematic of the first photostimulation frame of the bar-like photoactivation on the map of S1 barrels. P, posterior; M, medial. (E) Snapshots of the cortical surface illustrating bar-like photostimulation frames for each virtual cursor position. Only when the virtual cursor was in position 5, licks were rewarded. Same scale as in (D).

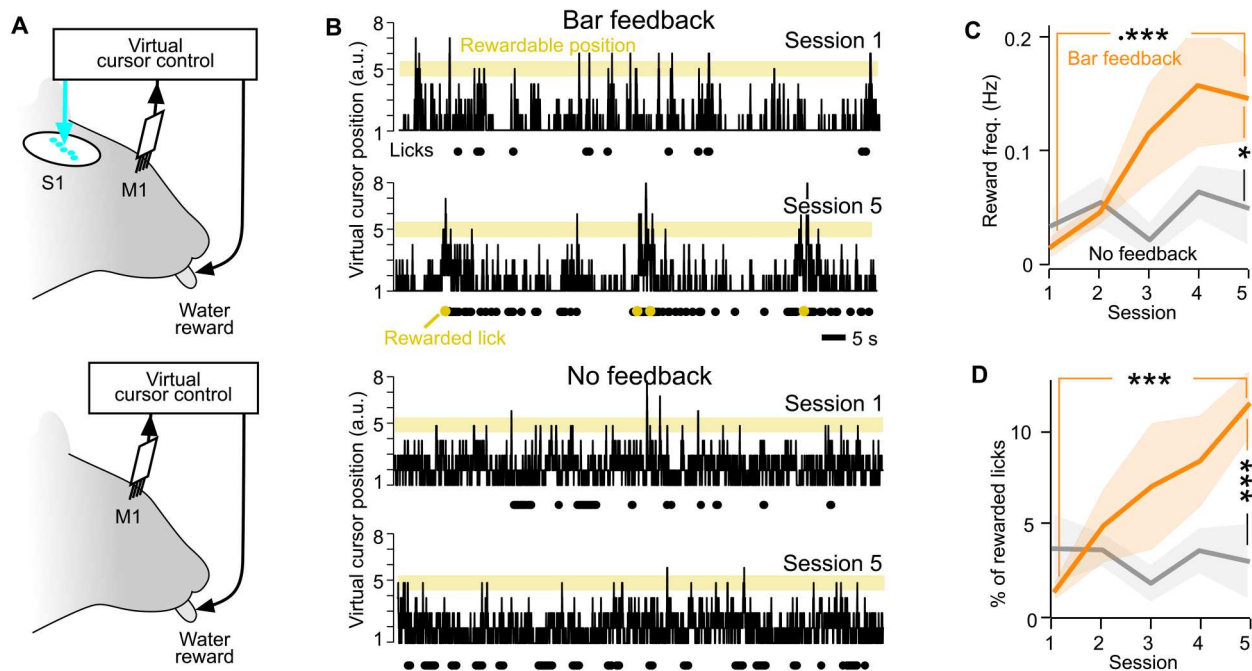


Fig. 2. Sensory feedback to the whisker part of S1 enhances task performance. (A) Schematic of the Bar feedback and No feedback conditions. (B) Position of the virtual cursor computed from the merged activity of the Master neurons, in the first versus the fifth training session of one mouse, in the Bar feedback condition (top) and in the No feedback condition (bottom) (100 s displayed). Yellow background, rewardable position; black dots, lick times; yellow dots, rewarded lick times. (C) Performance quantified by the average frequency of rewards per session across training, comparing the Bar feedback condition (orange, 10 mice) and the No feedback condition (gray, 8 mice). Shaded backgrounds: \pm SEM. * $P < 0.05$ and *** $P < 0.001$, nonparametric Mann-Whitney tests. (D) Same as (C) for the specificity of licking, quantified as the proportion of rewarded licks among all licks, across behavioral sessions.

divided by the duration of the whole 30-min session) and proportion of rewarded licks (measured over the course of the whole session).

On the first session, the mice licked occasionally but the virtual cursor was almost never in the rewardable position at the same time, and the mice obtained almost no water. On the fifth day training session, the same mice performed licking bouts at times when the virtual cursor entered the rewardable position, and thus obtained rewards more frequently. Overall, over the course of five training sessions, the performance measured as the frequency of rewards (licks per second) significantly increased more than 10-fold (from 0.014 to 0.19 rewards/s; orange curve of Fig. 2C; Mann-Whitney $P = 0.0010$, $n = 10$ mice). In contrast, in the absence of optogenetic feedback (Fig. 2, A and B, bottom), the mice failed to reliably increase the frequency of rewards despite the same amount of training (0.025 versus 0.022 rewards/s; gray curve in Fig. 2C; Mann-Whitney $P = 0.48$, $n = 8$ mice among the 10 tested in the Bar feedback condition).

The increased reward frequency in the Bar feedback condition was accompanied by an increase in the specificity of licking, measured by the percentage of licks that were rewarded among all licks (Fig. 2D; Mann-Whitney $P = 2.4 \times 10^{-4}$). This indicated that the mice did not simply increase their licking frequency irrespective of the virtual cursor position to solve the task. We conclude from these data that the optogenetic feedback to the barrel cortex was required for learning to control this brain-machine interface within five training sessions.

Shuffling the spatiotemporal structure of the feedback disrupts learning

We hypothesized that in these initial experiments, the specific spatiotemporal structure of the Bar feedback helped the mice to control the virtual cursor, whereas other types of feedback might not result in similar fast task learning. To explore this question, we selected a subset of three additional feedback conditions that degraded the spatiotemporal structure of the original Bar feedback in controlled ways (Fig. 3A).

In the Barrel shuffle condition, we degraded the spatial arrangement of the Bar feedback by randomly shuffling the identity of the photostimulated barrels, therefore removing the contiguity and spatial alignment between simultaneously activated barrels, but preserving temporal overlap of two to three barrels from one frame to the next (six mice; see all photostimulation frames in fig. S4). In the Frame shuffle condition, we preserved the spatial organization of the photoactivated barrels within one frame, while in contrast, the correspondence of the frames with the virtual cursor position was shuffled. This rearrangement disrupted the overlap and contiguity of the displayed frames during evolutions of the virtual cursor (six mice). Last, in the Full shuffle, both the spatial position of the barrels and the frame-to-cursor correspondence were randomized (eight mice).

We trained mice to control the virtual cursor by M1 neuronal activity while receiving these different feedback patterns. Apart from the spatial content of the optogenetic frames themselves, training was identical to that implemented for the Bar feedback and No feedback conditions. In these experiments, the mice remained

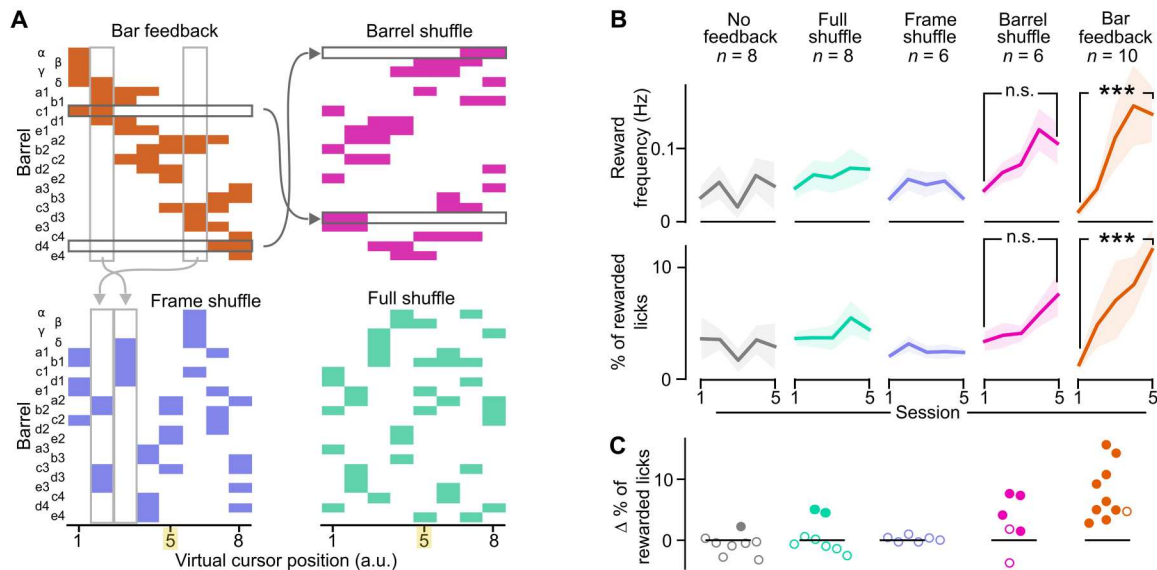


Fig. 3. Disrupting the spatiotemporal structure of the Bar feedback impairs learning. (A) Spatial and temporal structure of the feedback across frames in the four tested conditions. Horizontal arrows, barrel identity permutation to generate the Barrel shuffle from the Bar feedback; vertical arrows, frame identity permutation to generate the Frame shuffle from the Bar feedback; yellow highlight, rewardable virtual cursor position. (B) Reward frequency (top) and percentage of rewarded licks (bottom) of the mice over five training sessions. *** $P < 0.001$, nonparametric Mann-Whitney tests. n.s., not significant. Shaded backgrounds: \pm SEM. Bar feedback and No feedback data are the same as in Fig. 2. (C) Difference between the proportion of rewarded licks of the mice between the first versus fifth training session. Each point represents a mouse (arbitrary order). Filled point: bootstrap significance test, $P < 0.05$. Colors refer to the feedback conditions defined in (A).

actively engaged. They licked and obtained rewards throughout all training sessions (fig. S5A). However, in contrast to the Bar feedback condition, we found no significant increase in mice performance across sessions (Fig. 3B). In the Barrel shuffle condition, we noticed a trend toward an increase in the reward frequency and in the percentage of rewarded licks, but it did not reach significance (Fig. 3B; reward frequency: Mann-Whitney $P = 0.064$; % rewarded licks, $P = 0.132$), although four of six mice did show a significant increase in the percentage of rewarded licks (Fig. 3C). Note that the increase in performance revealed in the Bar feedback condition was still significant when the number of mice was reduced to six as in Barrel or Frame shuffle feedback conditions (Mann-Whitney $P < 0.05$ for any of the 210 possible combinations), excluding a mere effect of sample size.

Through these experiments, we consecutively trained mice to learn the task with multiple different feedback structures. Therefore, the order of the training sequence might have had an impact on the learning performance. We explored this potential effect with two groups of three mice, which followed consecutively training in the No feedback, Full shuffle, and Bar feedback conditions, in two different orders (fig. S5B). Irrespective of the protocol training order, significant learning was observed only in the Bar feedback condition (Mann-Whitney $P = 0.04$; see also table S1). In addition, a two-way analysis of variance (ANOVA) analysis of the impact of the feedback condition and the order of training revealed that the selected feedback contributes significantly to the observed performance variation ($P = 3.2 \times 10^{-5}$, sum of square = 0.039) but the order of training does not ($P = 0.24$, sum of square = 0.0011). We conclude that the feedback identity dominates over the order of training. Our data also indicate that the Bar feedback is required not only for learning but also for postlearning performance (fig. S5C). Overall, we found that the spatiotemporal structure of the

feedback affected heavily the behavioral performance of the mice and that the Bar feedback enabled fastest learning. Note that learning was only visible when looking at several consecutive training sessions, as we did not find evidence of within-session performance improvements (fig. S5D).

Mice learn to bring the virtual cursor in the rewardable position dynamically

Next, we asked which mechanisms could underlie the ability of mice to improve their performance over the five training sessions. Mice could adapt their M1 activity to bring the virtual cursor more often and/or longer in the rewardable zone, they could adapt their licking behavior to take advantage of reward opportunities, or they could adapt both M1 activity and licking behavior synchronously. We started by investigating possible changes in the dynamics of the virtual cursor. We analyzed these dynamics at different timescales, focusing on how it changes from the first to the fifth training session. First, we measured the average time spent in the rewardable position across the whole duration of a session (Fig. 4A). We found that it increased significantly in the Bar feedback condition (Mann-Whitney $P = 0.034$), in contrast to all other tested feedback conditions. In addition, in this feedback condition, we computed offline the virtual cursor positions corresponding to the 3-min baseline firing rate, and we found that only in session 5, it was significantly smaller than during the task. These observations confirm that in the Bar feedback condition, the mice learned to bring the cursor in the rewardable position more often. When we plotted the average virtual cursor position in time, first on a long timescale, we noticed that the curves for sessions 1 and 5 started at the same level, followed by an upward shift 10 to 15 s after the start of the photostimulation in session 5 (Fig. 4B; cursor position significantly

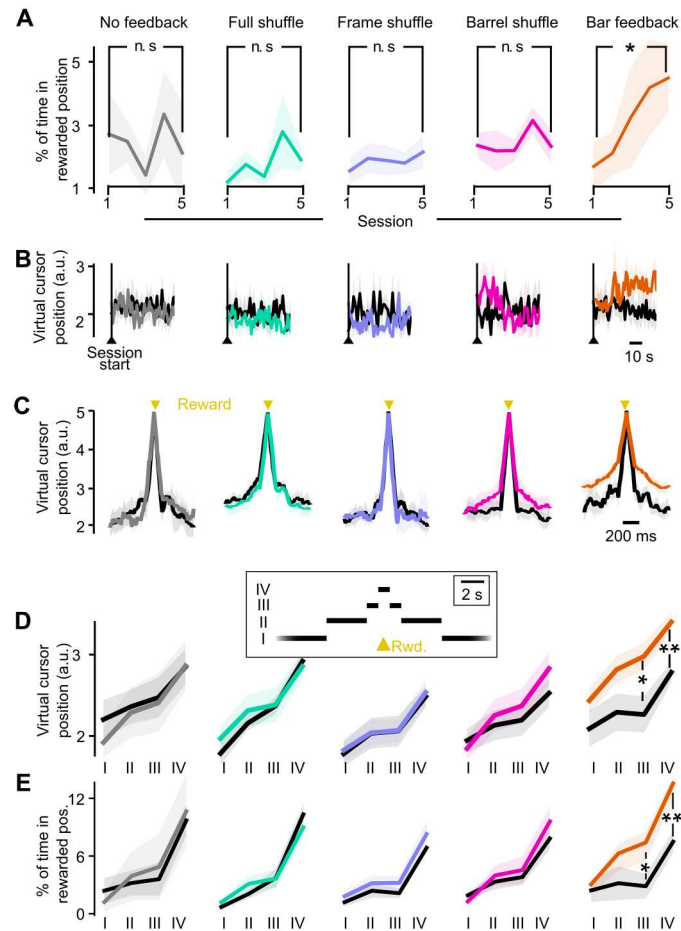


Fig. 4. Bar feedback enables the mice to actively control the virtual cursor position so that they spend more time in the rewardable position. (A) Proportion of time spent in the rewardable virtual cursor position (position 5) over the whole session duration. (B) Average virtual cursor position at the onset of the session, in the first versus last training session. Vertical line: start of the session, which is also the start of the photostimulation. (C) Average virtual cursor trajectory, aligned to the reward times, in the five feedback conditions. Black, first session; colors, session 5. (D) Average virtual cursor position, in four time windows around reward: (I) more than 5 s away from any reward, (II) 1.5 to 5 s away, (III) 0.5 to 1.5 s away, and (IV) within 0.5 s of a reward. Mann-Whitney, * $P < 0.05$ and ** $P < 0.01$. (E) Average percentage of time spent in the rewardable position, in the four time windows around reward defined in (D). For all panels: Light background: SEM across mice. Mann-Whitney, * $P < 0.05$ and ** $P < 0.01$. Colors refer to the feedback conditions defined in Fig. 3.

higher in 15 to 100 s versus 0 to 10 s; Wilcoxon test $P = 0.014$, only for the Bar feedback condition).

These delayed dynamics rule out the hypothesis that photostimulation could have nonspecifically increased the overall activity, and consequently the virtual cursor position. We then investigated whether there was a dynamical control of the virtual cursor on a faster timescale leading to rewards. We observed that in the Bar feedback condition, and only in this condition, the mean cursor position was significantly larger after training than on session 1, up to 1.5 s around reward occurrence (Mann-Whitney $P = 0.0044$ within 0.5 s of the reward, $P = 0.016$ in the time window 0.5 to 1.5 s around reward; Fig. 4, C and D). In the same time windows, the virtual

cursor spent a proportion of time in the rewardable position that was significantly larger after training compared to before (Mann-Whitney $P = 0.0031$ within 0.5 s of the reward, and $P = 0.045$ in the time window 0.5 to 1.5 s around reward; Fig. 4E). There were no significant changes in these measures in epochs further away from rewards (1.5 to 5 s and >5 s from any reward; Mann-Whitney $P > 0.05$), indicating that there was not a systematic additive shift in the virtual cursor position throughout the session. Rather, the cursor moved by numerous fast explorations, which typically involved a large range of the eight possible positions. In the Bar feedback condition after training, the mice spent significantly more time in virtual cursor positions above the rewardable one (positions 6 to 8) and visited significantly more virtual cursor positions around reward times (detailed in fig. S11). Note that with perfectly accurate control, the mice should not need to visit positions above the rewardable position 5. Nonetheless, all eight patterns of the Bar feedback could have contributed to the observed performance. Overall, these results suggest that during training, the mice learned to manipulate the virtual cursor and bring it in the rewardable position more often, thus creating more opportunities for enhancing their performance by well-timed licks.

One Master neuron dominates control of the virtual cursor

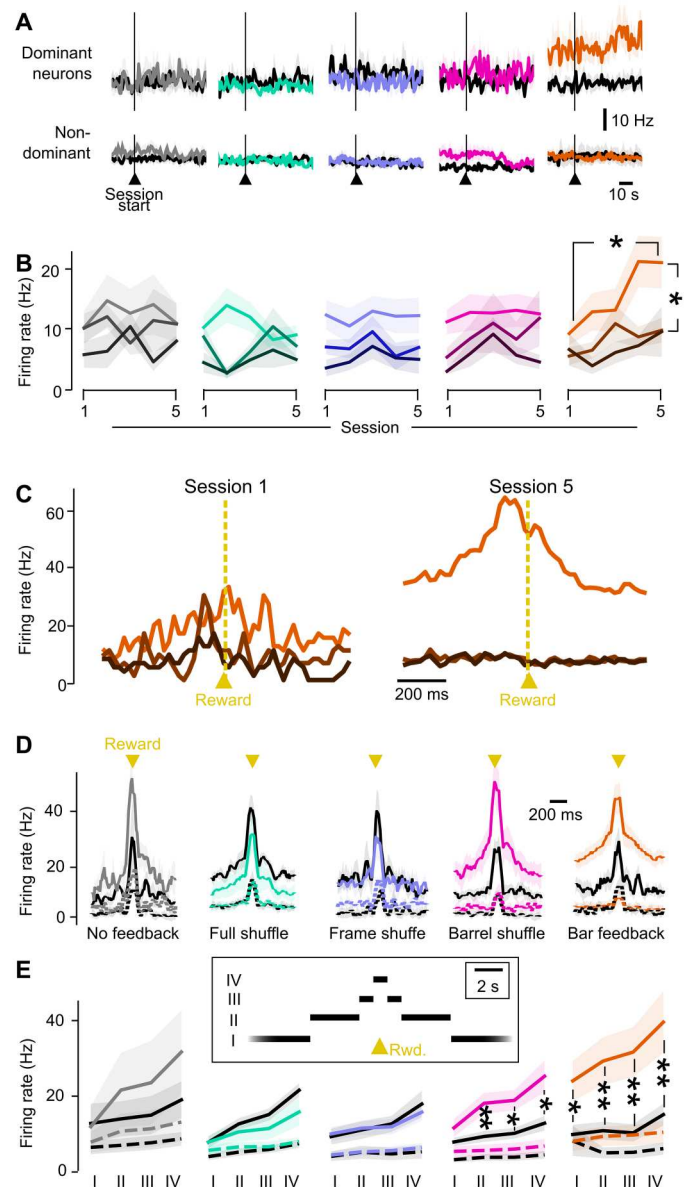
By design, changes in the dynamics of the virtual cursor are a direct consequence of changes in the underlying Master neuron activity, albeit in a nonlinear way tailored to each mouse extracellular recording (see Materials and Methods and fig. S3). We verified the changes in firing rate underlying the observed changes in virtual cursor trajectory. In particular, because the activity of several Master neurons was summed to drive the cursor, we wondered whether all Master neurons contributed equally, or if instead motor control of the virtual cursor was dominated by a subset of the Master neurons. To investigate this question, we sorted the Master neurons as a function of their contribution to the virtual cursor position at reward time, and we looked at the evolution of their spiking activity over training. We termed “dominant” the Master neuron that on average fired the most at reward time, in a ± 100 -ms window. Note that in the population analysis of Master neuron dominance, we focused on the three neurons that contributed the most to the summed Master firing rate even if, in two mice, up to seven Master neurons were involved in the control of the task.

First, we checked the firing rate of Master neurons at the time-scale of a whole session. Right at photostimulation onset, there was no detectable change of activity of Master neurons (Fig. 5A and fig. S9, B and C). This further indicates the absence of an immediate photostimulation effect, in agreement with what we had observed on the virtual cursor position (Fig. 4B; see also fig. S9A).

We noticed that in the baseline period before photostimulation start, the dominant Master neurons showed a markedly larger average firing rate in session 5 compared to session 1 in the Bar feedback condition (Fig. 5A). Note that this persistent elevation of firing before photostimulation is, by construction, normalized away by the control algorithm and thus does not contribute to changes in virtual cursor position (see Materials and Methods). This explains why the mean position was unchanged right at the beginning of session 5 compared to session 1 (Fig. 4B). After photostimulation, when averaged across the whole duration of session 5, the firing rate of the dominant Master neuron stayed elevated. It was significantly larger after training compared to before (Mann-Whitney $P = 0.011$) and

Fig. 5. Emergence of a dominant Master neuron in the Bar feedback condition.

(A) Firing rate at the onset of the session, for dominant (top) and nondominant (bottom) Master neurons in the first (black) versus last training session (colors). (B) Mean firing rate of the dominant and nondominant Master neurons. In (B) and (C), color saturation decreases from largest contributor to the firing rate at reward time (dominant Master neuron, bright color) to the second and third largest contributors (nondominant Master neurons, dark colors). Shaded backgrounds: \pm SEM across mice. (C) Mouse case study of the time histogram of the activity of Master neurons around rewards, in the Bar feedback condition, sorted from the weakest (dark brown) to the dominant neuron (saturated orange) at the time of the reward, in the first (left) versus the fifth (right) training sessions. (D) Time histogram of the activity of Master neurons around rewards, in the five tested feedback conditions. Session 1 is shown in black, and session 5 is shown in saturated colors. Continuous line, dominant Master neuron; dashed line, average of nondominant neurons. (E) Average firing rate of dominant (continuous line) and nondominant (dashed line) Master neurons in the first (black) versus the last training session (colors), measured in the same time windows as in Fig. 5: (I) more than 5 s away from any reward, (II) 1.5 to 5 s away, (III) 0.5 to 1.5 s away, and (IV) within 0.5 s of a reward. For all panels: Shaded backgrounds: \pm SEM across mice. Mann-Whitney, * $P < 0.05$; ** $P < 0.01$. Colors refer to the feedback conditions defined in Fig. 3.



larger than the firing rate of nondominant Master neurons (Fig. 5B; Mann-Whitney $P = 0.017$; see also fig. S6E). This increase was specific to the Bar feedback condition. Thus, Bar feedback training resulted in an elevation of firing not only in the baseline period but also on the long timescale of the session duration. On the contrary, nondominant Master neurons (Fig. 5, A and B) and neighbor neurons (fig. S6D) showed little change in activity upon behavioral training. In parallel, we found a significant increase in the SD of the firing rate of the dominant Master neurons (detailed in fig. S6F), confirming the specificity of their modulation compared to nondominant neurons. We did not find that Master neurons with a high firing rate in session 1 were the ones that increased their firing rate the most in session 5 (fig. S6C, also shown for neighbor neurons). The same analysis showed that four of the six dominant Master neurons that we could track across the five training sessions were not dominant in all five training sessions. We hypothesize that

this is due to the fact that the dominant Master neuron had not yet fully emerged during the first 3 training sessions.

Next, we asked how the dominant Master neurons modulated their activity on a shorter timescale around rewards, similar to the way we looked previously at the virtual cursor position (Fig. 4C). Figure 5C shows the firing rate of individual Master neurons around reward times, for sessions 1 and 5 of one mouse trained in the Bar feedback condition. After training, one of the Master neurons showed a much higher firing rate with a prominent peak around the reward time. Population averages across mice confirm this tendency for the dominant neuron in the pool of Master neurons, whereas little changes were observed on nondominant neurons (Fig. 5D). Again, this was specific to the Bar feedback condition, although a more moderate trend was also noted for the Barrel shuffle condition. We quantified the firing rate in several time windows around rewards (similar to Fig. 4D for the virtual

cursor position). The firing rate of dominant Master neurons around reward times in the Bar feedback condition showed a strong and significant increase after training compared to before (Fig. 5E). This increase was specific to the dominant Master neurons and was highest around reward times (Mann-Whitney $P < 0.01$). It was less pronounced but still significant more than 5 s away from any reward (Mann-Whitney $P = 0.04$), an observation that we relate to the elevated firing rate in the baseline period already before the task started (Fig. 5A). We observed a similar but more limited phenomenon in the Barrel shuffle condition (Fig. 5E). Overall, we conclude that in the Bar feedback, and to a lesser extent in the Barrel shuffle, the mice learned to control the virtual cursor position mostly by increasing the activity of one Master neuron in bursts of elevated firing around lick times, enabling them to obtain rewards.

Mice learn to lick during time windows of reward availability

Beyond the observed changes in M1 neuronal activity, the mice may also optimize their licking strategy to obtain more rewards. When looking at the overall licking statistics in the first 10 min of the sessions, during which the mice were most active, we found that over the course of training, they increased significantly their licking rate in the Bar feedback condition (Fig. 6A, top; Wilcoxon $P = 0.037$), as well as in the Full shuffle condition (Wilcoxon $P = 0.023$). In addition, specifically in the Bar feedback condition, the SD of the licking rate (measured in consecutive 1-s bins) increased significantly (Fig. 6A, middle; Wilcoxon $P = 0.0137$), and the mean interval between

consecutive lick bursts decreased significantly (Fig. 6A, bottom; Wilcoxon $P = 0.0097$).

These results indicate that the mice learned to lick overall more and in closely spaced bursts, thus increasing their chances of obtaining rewards. These changes in licking statistics may be accompanied by an increased coordination of licking with the entries of the virtual cursor in the rewardable position, as it would further ensure larger amounts of rewards. To explore this hypothesis, given the tendency of mice to lick in long rhythmic bursts, we focused on the onsets of licking bouts (Fig. 6B). We computed the proportion of lick burst onsets that fell within ± 100 ms of the virtual cursor entry in the rewardable position, which is approximately the duration of a tongue licking cycle. We found that this proportion increased significantly only in the Bar feedback condition (Fig. 6, C and D; Mann-Whitney $P = 0.0028$) and that a similar, nonsignificant trend was visible in the Barrel shuffle condition. We conclude from these data that the mice did learn to modify their licking patterns and adjust them to the virtual cursor dynamics.

Playback experiments confirm the role of active motor control for task performance

Last, to further explore the role of motor control on task performance, we performed playback experiments on three mice that had already learnt the full closed-loop task with the Bar feedback protocol. The mice received the same optogenetic stimulation sequence as in their last closed-loop session with Bar feedback, and they could still receive reward by licking when the virtual cursor was in the rewardable position. However, the virtual cursor dynamics was now independent from the ongoing activity of motor cortex

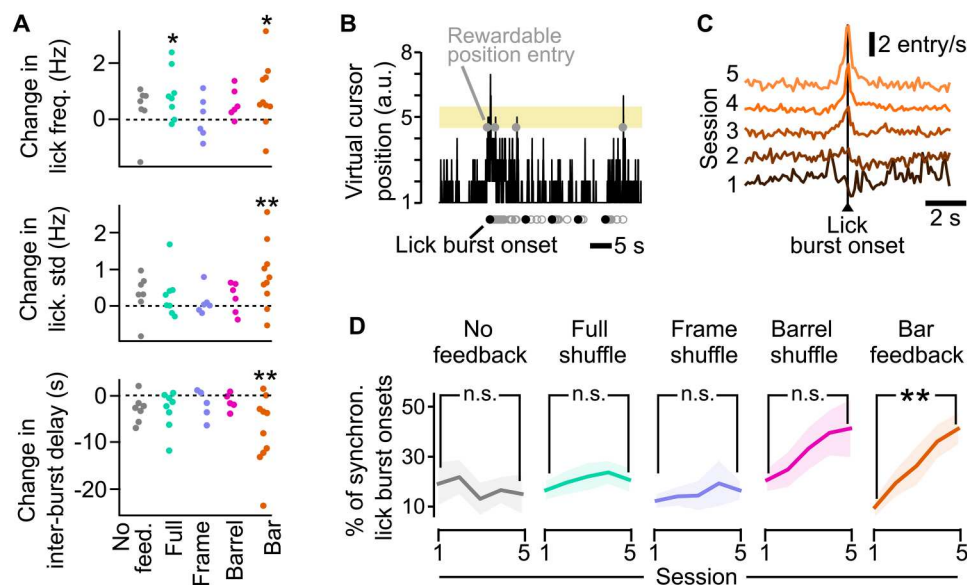


Fig. 6. Evolution of licking with learning and emergence of a synchronization between licking and entries of the virtual cursor in the rewardable position. (A) Evolution of the licking pattern between the first and fifth training session in the first 10 min of the task. On each graph, one point represents one mouse. Top, change in the licking frequency; middle, change in the SD of the licking frequency measured in 1-s bins; bottom, change in the delay between two bursts. Wilcoxon test, * $P < 0.05$ and ** $P < 0.01$. **(B)** Example of the virtual cursor position as a function of time. Gray open circles, licks; black dots, onsets of lick bursts. Gray dots on virtual cursor position 5 indicate entries of the virtual cursor in the rewardable position. To avoid confusion, rewarded licks are not highlighted. **(C)** Population average time histograms of the number of entries of the virtual cursor in the rewardable position around all lick burst onsets, for the Bar feedback condition, across the five training sessions. Baseline levels were shifted upward for clarity. **(D)** Percentage of lick bursts that are synchronous (within ± 100 ms) with entry of the virtual cursor in the rewardable position. Mann-Whitney, ** $P < 0.01$. For all panels: Shaded backgrounds: \pm SEM. Colors refer to the feedback conditions defined in Fig. 3.

neurons. In other words, the animals were relieved of the motor control aspect of the full task (Fig. 7, A and B). The median frequency of rewards dropped significantly in the playback condition (Kruskal-Wallis, $P = 0.0495$; Fig. 7C) even though, by design, the virtual cursor spent as much time in the rewardable position as during the Bar feedback last session. Analysis of the synchrony between licking onsets and the entries of the virtual cursor in the rewardable position revealed that these events were not coordinated anymore (Fig. 7D). There was no correlation with whisking either (fig. S10).

To confirm that active motor control is necessary not only for task execution but also for learning, we trained three naïve mice to perform the playback task during five sessions. Consistent with the previous playback result, we found that the mice failed to increase significantly their performance during this playback training (fig. S7). Overall, these playback experiments demonstrate that in the Bar feedback condition, the mice did not only respond to sensory cortex stimuli by licking, but instead actively coordinated their licking with timely modulations of the cursor position.

DISCUSSION

In this study, we demonstrate that in the context of improving motor control of a brain-machine interface, the integration of direct cortical feedback can be heavily affected by its spatiotemporal organization. Specifically, we trained mice in a task for which the

brain-machine interface could be used to move a virtual cursor into a rewardable zone. We found that the performance after training was highest when feedback provided the position of the cursor in the form of a bar-like photostimulation across the cortical surface (Bar feedback condition). In contrast, we found that when we disrupted the spatial contiguity of simultaneously stimulated barrels (Barrel shuffle), learning was clearly reduced, and when we disrupted the continuity of the bar in time (Frame shuffle), it went down to levels observed without feedback.

This difference in performance was associated with a reorganization of the ongoing neuronal activity that was specific to the Bar feedback condition. More precisely, one of the M1 Master neurons driving the cursor became dominant in terms of activity levels and led the virtual cursor to spend more time in the rewardable position, thereby increasing the opportunity for rewards. In parallel, licks were more synchronized with entries in the rewarded position.

A fast bidirectional brain-machine interface setup for the mouse

Current research aimed at integrating somatosensory feedback in a cortical brain-machine interface relies on invasive techniques of recording and stimulation in awake behaving animals. Pioneering teams are developing prototypes in nonhuman primates as well as human participants (8, 9). Here, we have developed a brain-machine interface tailored to the mouse whisker system, a sensorimotor loop that has been described in a comprehensive way, from

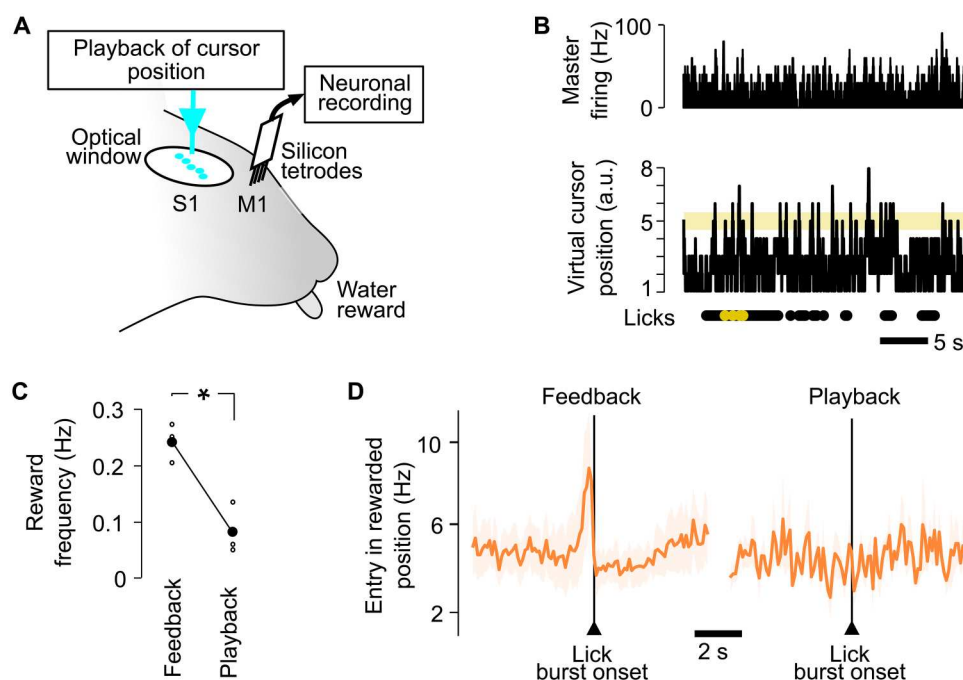


Fig. 7. Lick timing is not accurate in a playback condition. (A) Playback configuration with chronic extracellular recording in M1 and Bar feedback optogenetic stimulation on barrels in S1. Previously acquired sequences of cursor positions are played back, independent from M1 firing rates. As in closed-loop sessions, reward delivery is contingent on synchronous (i) licking and (ii) presence of the virtual cursor in the rewardable position. (B) Top: Histogram of Master neuron activity during a playback session (30 s shown). Bottom: Time course of the virtual cursor position, disconnected from the Master firing. Below: Licks and rewarded licks during the same interval. Bin size, 10 ms. (C) Frequency of rewards during the last session with closed-loop Bar feedback (session 6 after the standard five training sessions; table S1) and the session with open-loop Bar playback that followed on the next day. Kruskal-Wallis, $*P < 0.05$. Gray background: SEM. $n = 3$ mice. (D) Histogram of lick burst onsets, with respect to the times of entry of the virtual cursor in the rewardable position around the onset of lick bursts, for the last session with closed-loop Bar feedback (left) versus the session with open-loop Bar playback (right), averaged for the three tested mice.

the cellular to the network level (21, 22). This approach has allowed us to take advantage of recent optogenetic tools available for these animals. We could activate excitatory neurons in the cortex according to spatial light patterns that were adapted, in each individual mouse, to the topographic map of the whiskers present in S1. Furthermore, we benefited from our low-latency (12 ± 5 ms) closed-loop design, which enables the delivery of feedback in a dynamic way so that the ongoing activity of the Master neurons controlled online the stimulation frames. A low-latency somatosensory feedback could be an important parameter in the context of sensorimotor learning (31).

To provide distributed feedback to the mice, we chose to generate illumination patches above individual S1 barrels, rather than try to mimic the broad spread of activity that is generated by multiple whisker stimulation sequences (27). The rationale has been to mimic activation patterns of multiple lemniscal thalamic inputs, which are known to project into barrel columns of corresponding whiskers, and which should then trigger broader activation of the cortex through intracortical connectivity, both within and across layers (22). We hypothesize that this recruitment of intracortical mechanisms is key to the similarity between artificial and physiological stimulation. We certainly acknowledge that substantial differences remain between the optogenetic activation and physiological activation of the barrel cortex. In particular, we did not attempt to reproduce nonlemniscal thalamic input patterns, which do not follow a clear topographical mapping at the surface of the cortex, and which are thus difficult to activate specifically.

Impact of somatosensory feedback on neuroprosthetic learning

In our experiments, in the absence of optogenetic feedback, the mice failed to learn the task. In contrast, a few previous studies have suggested that brain-machine interface learning could take place without any feedback of the conditioned neuronal activity to the animal (32, 33). Several differences could explain these seemingly opposite results. First, in those studies, the animals received the reward automatically once the neuronal activity reached the pre-defined threshold. In contrast, in our task, the mice have to learn also to lick to obtain the reward. This combination of firing rate modulation and required licking probably makes the task much more challenging. Second, in our study, movements of the virtual cursor occurred on average every 50 ms so that temporal precision of licking was important. This must also have been challenging, particularly in the absence of any feedback. These reasons could explain the lack of learning that we report in the No feedback condition.

Our study shows that direct cortical feedback can enable the learning of a sensorimotor task in these conditions, pending that feedback with an adequate spatiotemporal structure is provided. This is consistent with recent work exploring cortical somatosensory closed-loop brain-machine interfaces in humans with intracortical electrical stimulations (8), as well as with previous work emphasizing the prevalent role of ongoing sensory feedback in motor learning (31, 34).

Our experimental design did not incorporate a physical implementation of a device to be moved by the animal toward a target. Instead, we computed the position of a virtual cursor and used it to select the next frame of the ongoing feedback. This choice ensured that the optogenetic feedback delivered to S1 was the sole source of sensory information about the virtual cursor position available to

the animal during the task. This is in contrast to most previous closed-loop brain-machine interface studies, in which ongoing visual feedback of the neuroprosthesis was always available for adjusting motor control in addition to cortical stimulation (8, 9).

Motor control of the virtual cursor

In this study, direct demonstration of voluntary motor control was challenging because virtual cursor movements were generated continuously rather than triggered. Still, we found several indications of active motor control of the virtual cursor, which were specific to the Bar feedback condition and, to a lesser extent, to the Barrel shuffle condition. In particular, only in this feedback condition did the virtual cursor position shift toward the position of the rewarded frame, as the mouse prepared to collect rewards in the next seconds (Fig. 4, C and D, and fig. S11). In addition, analysis of the neuronal activity of the Master neurons underlying the virtual cursor position revealed that throughout learning sessions, neuronal activity evolved toward the dominance of a single one of the Master neurons, in particular during the modulations of activity toward the rewarded position. This rearrangement took place only in the Bar feedback condition (Fig. 5). Last, during additional playback sessions at the end of a sequence of training in the Bar feedback condition, the mice appeared unable to maintain the performance level they attained during previous closed-loop training sessions, indicating that active motor control was required for performance (Fig. 7).

Overall, we conclude from our data that in the Bar feedback condition, the mice did rely on the active modulation of the Master neurons to collect rewards. The lack of such motor control in other feedback conditions illustrates the impact of the spatiotemporal structure of our distributed feedback, not only for sensory information processing but also more generally for sensorimotor integration of the feedback.

Regarding the playback experiments, we should point out that in one study, after operant conditioning of motor cortex neurons based on a single barrel S1 optogenetic feedback, mice were able to efficiently gather rewards during playback training (16). Similarly, we have previously shown that in our experimental setting, mice were able to detect a static, single frame of the Bar feedback to obtain rewards (15) or to track a continuous, slowly rotating bar (35). We hypothesize that what makes the playback condition here (Fig. 7) comparatively more challenging than during these previous experiments is that it combined rapidly changing feedback with a distributed, more complex spatial pattern. In addition, a low-latency licking was necessary when the cursor entered the rewardable frame. All these challenges meant that to be successful, the mice had to anticipate the entrance in the rewardable frame, as the cursor could escape the rewarded position within milliseconds. In contrast to the playback condition, we hypothesize that in the closed-loop Bar feedback condition, the motor control of the virtual cursor provided the degree of rewarded frame anticipation that allowed timely licks and an increase in the proportion of rewarded licks. Overall, it appears that due to the fast-paced nature of the required behavior, the mice could only achieve accurate licking by combining motor control of the virtual cursor with online cursor feedback.

Pattern contiguity affects learning and performance

So far, the contribution of cortical maps to sensory information processing in general has remained unclear (36) despite the thorough descriptions of the maps in primary sensory cortices. In the case of the barrel cortex, several of the functional properties encoded by its neurons are spatially organized inside the map beyond spatial topography (37–40), including some multiwhisker features (27, 38). This topographical organization provides a rich anatomical substrate for nonlinear spatiotemporal integration in S1, which results in enhanced or suppressed responses to specific distributed input patterns (41). However, so far, these feature extraction properties have not been causally linked to behavior, except recently for the somatotopy itself in the context of a discrimination task (35).

Here, we show that the spatiotemporal organization of distributed feedback at the surface of a topographical cortex can have a large impact on motor control. Specifically, we found that the mice were able to learn to control a virtual cursor using an S1 bar-like feedback that featured contiguity of the activated barrels both within a given frame and across consecutive frames.

When across-frames contiguity was removed, in the Frame shuffle feedback condition and also the Full shuffle condition, we found no sign of learning, as in the absence of feedback altogether. We hypothesize that the lack of temporal continuity across consecutive feedback frames may have prevented the anticipation of upcoming cursor movements. Given our fast-paced cursor positioning task, this translated in an inability to learn the task. This hypothesis is consistent with the findings in our previous open-loop discrimination task (35).

However, when only within-frame contiguity was removed (Barrel shuffle condition), learning was at intermediate levels. The mice were able to exploit the feedback to some degree but lacked the accuracy that is required to synchronize virtual cursor and licking efficiently. These results on the relevance of both the spatial and the temporal structure of intracortical feedback suggest that the sensorimotor task of driving the virtual cursor to the target draws upon preexisting features of S1-M1 microcircuits, linked to their topographic organization (42). When the contiguity of the feedback was disrupted, the functional architecture of the cortex may not have been adapted anymore to the novel sensorimotor computations that were required to solve the task. Thus, learning to extract the relevant virtual cursor information from the different shuffled conditions may require multiple additional training sessions, if indeed the required functional connections can be recruited from the existing anatomical scaffold (43). Previous work does suggest that learning a spatially shuffled cortical stimulation is possible if training spans multiple training sessions, with the assistance of visual feedback (19, 44). This seems consistent with the signs of learning that we did observe in the Barrel shuffle condition (Fig. 3, B and C).

Neuronal substrate of the selectivity to distributed patterns

In previous studies, we performed control experiments during which we recorded activity in S1 during bar-like stimulations [figure S1 in (35)] and single-spot photostimulations [figure 4 in (15)]. These experiments suggest that there is no artifactual, oversized response of S1 neurons to the Bar feedback patterns compared to single-spot photostimulations.

However, beyond this basic control, it is unclear whether the specific success of the Bar feedback condition in our sensorimotor task entirely stems from the inter-area connectivity in the sensorimotor loop or whether it builds mostly on processing that would take place in the local microcircuits of S1. Several recent studies have used two-photon imaging to measure the activity of neurons in primary sensory areas during detection of a spot-like optogenetic photostimulation. One study showed that over the course of training sessions, an optogenetic spot stimulation in S1 increasingly engaged the touch-related neuronal assemblies in this area, disproportionately more than the whisking-related neurons (45). In another study focusing on the primary visual cortex (46), neurons recorded in the cortical area below the stimulation spot developed a specific tuning for the single spot compared to other stimulation patterns.

On the basis of these findings, we hypothesize that part of the selectivity to our Bar feedback patterns could arise from plasticity internal to the S1 microcircuit, accompanied by other changes in the S1-to-M1 connectivity. Additional experiments will be required to tease out these mechanisms more precisely for such complex, spatially and temporally structured photostimulations across several training sessions.

Plasticity of sensory and motor cortical circuits

Similar to classical skill learning, brain-machine interface learning is thought to engage plasticity of neuronal circuits, including Hebbian plasticity of neuronal connections. In our study, because of the direct interfacing with the somatosensory cortex on the input side and the motor cortex on the output side, we expect changes in connectivity within and between these cortical areas, in addition to changes in more distant areas (47). In S1, as discussed above, the optogenetic feedback patterns that were most efficient were those exhibiting most spatiotemporal contiguity. This brings to mind the observation that, at the peripheral level, spontaneous behavior results in multiwhisker patterns with marked contiguity in spatial and temporal properties. Awake behaving rodents actively generate deflections predominantly in sequences of several nearest-neighbor whiskers, with a predominance of rostrocaudal sweeps, while noncontiguous sequences are much less frequent (48). Resulting primary sensory cortical activity patterns are thus more likely to resemble those evoked by optogenetic Bar feedback patterns than by shuffled patterns. In turn, naturally coactive cells most likely developed strong connections between themselves and onto downstream neurons, shaping the neuronal circuitry within S1 and from S1-to-M1 to encode behaviorally relevant sensory features (26–28). Such plasticity mechanisms during the establishment of whisker perception could explain why in our study, naturalistic feedback such as the Bar feedback was more efficient for learning the closed-loop S1-to-M1 task. Because the mice did not adapt to shuffled feedback patterns on the timescale of the experiments, our study suggests that plasticity mechanisms within S1 may not have contributed substantially during task learning.

By contrast, on the motor side, we observed that the animals were able to readily adapt to the constraints that were present, on the timescale of the experiments. Consistent with previous studies (16, 29, 49, 50), we found that M1 neurons could be conditioned in an operant way to learn to control a virtual cursor along one dimension. At the end of training, only one of the M1 Master neurons appeared to carry the task-related modulations (Fig. 5). This suggests that because we selected randomly three neurons, those neurons

were not likely to naturally covary, and therefore learning synchronous modulation of the three neurons could have been too challenging, requiring the exploration of activity patterns that were not normally explored (51). There is evidence that as the number of neurons controlling motor brain-machine interfaces increases, it becomes necessary to take into account their initial functional connections in order to learn to control the prosthesis rapidly (51–53).

Overall, our results support previous studies suggesting that novel skill learning engages adaptive plasticity in cortical circuits, albeit within existing limits to neuronal adaptability. In particular, as has been argued before, the primary sensory cortical circuits may be intrinsically less plastic than motor circuits during motor skill learning (54). Future experiments will need to address this question, in particular via recordings of neuronal activity of S1 activity across successive behavioral sessions.

Outlook

Our results strongly support a functional role of topography of the somatosensory cortical map in the behaving animal, by testing causally the impact of different patterns of sensory input. In particular, our work reveals that within the topographical organization of the barrel cortex, feedback patterns that are contiguous are best suited to sensorimotor integration. Such optimal patterning of dynamical distributed feedback could be combined with other means of transmitting feedback information to the brain, such as temporal and amplitude modulation of stimulation pulses (14, 16, 55).

Last, current brain-machine interface prototypes require long training and lack precision and flexibility, probably because they lack the appropriate somatosensory feedback (56). From our results, we propose that feedback strategies based on intracortical stimulation should favor spatial and temporal continuity within the known topography of the target areas. We hope that unveiling such fundamental constraints of neuronal circuits will enable the development of a new generation of brain-machine interfaces, incorporating rich proprioceptive and tactile feedback essential to achieve dexterity and embodiment.

MATERIALS AND METHODS

Mouse preparation

All animal experiments were performed according to European and French law as well as CNRS guidelines and were approved by the French ministry for research (Ethical Committee 59, authorization 858-2015060516116339v5 and 25932-2020060813556163v7). The data were obtained from 16 adult (6 to 10 weeks old) *Emx1-Cre;Ai27* mice (30). The brain-machine interface methodology has been published previously (15). All surgeries were performed under isoflurane anesthesia in 100% air. Isoflurane concentration was adjusted in the range of 1 to 4% depending on mouse state, assessed by breathing rate and response to tail pinch. Each mouse underwent two surgeries. During the first surgery, a 5-mm-diameter glass optical window was implanted over the left primary somatosensory cortex [S1, posterior: -1.5 mm and lateral: 3.3 mm from the bregma; (57)], and a head-fixation bar was implanted on the contralateral side of the skull (58). Eight days later, the clarity of the optical window was assessed, and if adequate, intrinsic imaging was performed to locate the S1 barrels (see below). If this first step was successful, a second surgery was performed to chronically implant (59) a 32-channel silicon probe in the shape of eight

tetrodes (A4x2-tet-5mm-150-200-121-CM32, NeuroNexus, USA; Fig. 1, A and B, and figs. S1 and S2). The electrode was implanted in the whisker zone of the motor cortex (M1, anterior: 1.5 mm and lateral: 1.2 mm from bregma; electrode recording sites, 650 to 800 μ m deep in the cortex).

Chronic neuronal recordings

Following the second surgery, mice were monitored for 5 days to allow the extracellular recordings to stabilize (bandpass, 1 to 6000 Hz). We then characterized the shape and amplitude of the units isolated by the online spike sorting (Blackrock Microsystems, USA). Clusters corresponding to well-defined single units (consistent spike shape and an adequate autocorrelogram, with a clear refractory period, see Fig. 1B) were manually selected within the tetrode spike amplitude space. This manual selection was controlled before each session to ensure that we maintained unit separation while keeping track of the same units across sessions (fig. S1). Once the online spike sorting was ready, the training session began. At the start of the training sessions, we recorded a median of 25.5 neurons simultaneously, with an interquartile range (IQR) of 5.25 neurons ($n = 10$ mice). After 17 days (average last training session), we recorded a median of 25 neurons (IQR = 16 neurons, $n = 10$ mice).

Brain-machine interfacing

Among the recorded units of each mouse per session, a set of three putative pyramidal neurons—the Master neurons—were selected by the operator. In the first two mice, we initially enrolled seven neurons. However, after the first round of experiments, we found that securing so many large and high-firing neurons was challenging in several of the mice, so we settled on a smaller count of three neurons. We did not find any major difference in the activity or behavior of these first two mice. We selected the Master neurons among all simultaneously recorded units because they displayed (i) a sufficient baseline frequency (target: 10 Hz), (ii) spikes clearly separate from the multiunit baseline and with the largest possible amplitude, and (iii) a spike shape that was visually different from any other spike shape across the four channels of the tetrode. The basic statistics of the Master neurons, including their mean firing rate and the SD over training sessions, are shown in fig. S6. In these panels, we also show the firing statistics of the neighbor neurons, defined as non-Master neurons.

The activity of these Master neurons was transformed into a virtual cursor position (Fig. 1C), which determined the optogenetic frame to be displayed as well as possible reward delivery. The spiking activity of the Master neurons was summed, and the corresponding firing rate was measured over 10-ms time bins. To transform this Master firing rate into the position of the virtual cursor, it was convolved with a 100-ms box kernel and then renormalized with respect to the distribution of Master activity observed during a baseline window of 3 min just preceding the start of the session. Specifically, we computed the 99th percentile of the baseline activity values, and the activity from 0 Hz up to this value was split in seven equal positions, with an additional eighth position for activity values exceeding the 99th percentile threshold (fig. S3). The resulting movements of the virtual cursor were smooth. In the Bar feedback condition, on average, 95% of the transitions were to a closest neighbor position, and less than 0.1% of the transitions were jumps

larger than to a second neighbor position. This was similar in all other feedback conditions.

For most of the experiments, only the fifth position was rewarded, which means that whenever the virtual cursor was inside that position and the mouse simultaneously licked, it obtained a water drop of volume 5 μl ($\pm 10\%$). Note that rewards were not delivered automatically to the mouse whenever the virtual cursor entered the rewardable position. Instead, only if the mouse licked at the precise time when the virtual cursor was located in the rewardable position, the capacitive sensor detected the lick and triggered the delivery of a drop of water through the lick port, which was immediately swept away by the ongoing licking action. In the very first three experiments, only the sixth position was rewarded, and in three additional experiments, the rewardable position also included either the sixth or the fourth position. We did not find any difference in activity or behavior that could be related to this difference in rewardable positions.

The logic of introducing a virtual cursor has been doubled. First, from a purely analytical point of view, it allows analysis of motor control in the nonlinear discretized scale that is relevant for feedback stimulation and reward obtention, that is, regardless of the absolute values of firing rates, which can be very different from one mouse and session to the next. Second, it emphasizes that the algorithm is the same in all feedback protocols. Only the final mapping between the eight different positions of the cursor and the effective photostimulation patterns changes with the protocol. This concept of a virtual cursor, in between the firing rate of the neurons and the photostimulation frames, is useful to describe unambiguously the protocols, the analyses, and the results.

Optogenetic photostimulation of somatosensory cortex

Each virtual cursor position was associated with a specific feedback pattern that was projected onto the barrel cortex of the mice using a Digital Light Processing (DLP) module (Vialux V-7001, Germany). The DLP contained a 1024×768 pixel Texas Instruments micro-mirror chip, which was illuminated by a high-power 462-nm blue light-emitting diode. The frame stream generated by the device was focused onto the cortical optical window using a tandem-lens microscope (60) and covered the entire barrel cortex. We displayed each frame for 5 ms, followed by 5 ms without photostimulation. This 50% duty cycle was selected to minimize channelrhodopsin desensitization resulting from permanent photoactivation (61). We sent homogeneous light spots, 225 μm in diameter, with an intensity of 20 mW mm^{-2} , centered onto the barrel locations (see next section). We chose this high intensity to trigger without a doubt a strong activation of the barrel cortex while still avoiding levels that could induce epilepsy. In a previous publication, we recorded activity in S1 in response to the exact same photostimulations, in the same mouse line, and verified that it triggered neuronal activation mostly limited to the targeted barrel area (15). In the same study, we also compared the detection of five aligned spots flashed on the barrel cortex to the detection of five aligned spots flashed just outside the cranial window, in a GO/NOGO task. We found that mice detected the photostimulation only when it was targeted to the cortical window. This control ensured that the mice are unable to use any indirect clue, such as light reflection in the setup, to solve the task.

A set of at least three reference barrels was localized on the mouse cortical surface via intrinsic signal imaging. These barrels

were used to align a standard barrel map (62) that served later as the grid to align the photostimulation spots. Figure S8 shows an example of the intrinsic signals and of the strategy used to position the photostimulations onto the S1 surface.

We used five different sets of feedback frames: the Bar feedback (Fig. 1, D and E), three shuffled versions of the Bar feedback that are described in Fig. 3 and fig. S4, and, finally, a condition where no photostimulation was displayed (No feedback, all black frames). The Bar feedback design was based on the known selectivity of S1 neurons to features such as the global direction of bar-like stimulations (26, 27, 63) and, more broadly, tuning to progressive movement of objects across the whiskerpad (28). This choice of feedback structure was also supported by the observation in awake behaving rodents that structured sweeping sequences of rostrocaudal deflections of whiskers are significantly more prevalent than expected by chance (48). Note that all photostimulation frames used the same number of identically shaped photostimulation spots and therefore generated the same amount of photoactivation (15). The total amount of light projected onto the cortex was thus constant throughout all sessions.

To verify that the selected photostimulation did not bias the M1 activity before training, we exposed three naïve mice to one single session of Bar feedback playback and one session of Full shuffle playback. The frame sequence originated from a previous mouse/training session. During playback, in each mouse, we recorded three M1 neurons that would qualify as Master neurons. We found no firing rate modulation triggered by any of the displayed frames (fig. S9A) and, in particular, none in the Bar feedback. These experiments, as well as similar analysis carried out for Master neurons in mice trained in the Bar and Full shuffle feedback conditions (fig. S9, B and C), confirm that before training, M1 neurons had no discriminative power or specific tuning to the photostimulation frames that we designed.

Behavioral training

We started the behavioral training by removing free access to the water in the cage. At the same time, we started habituating the mice to head fixation. This lasted for 2 days, where the mice were head-fixed during 30-min sessions and were continuously presented with a spout that delivered a drop of water every time the mice licked, owing to a capacitive sensor in the spout. To eliminate artifactual double detections that sometimes happened with the sensor, any detection that occurred less than 120 ms after a lick was dropped from further analysis.

After these first habituation sessions, we transitioned to training the mice in the brain-machine interface task. The sessions took place once a day and lasted 33 min (including the 3-min baseline period). During these training sessions, the neuronal activity was continuously recorded, and one of the five photostimulation dynamical patterns was continuously applied to the mouse barrel cortex: Bar feedback, Barrel shuffle, Frame shuffle, Full shuffle, or No feedback (Fig. 3A and fig. S4). The displayed frame was updated every 10 ms based on the measured neuronal activity (Fig. 1). At any time, the mice could move the virtual cursor to the rewardable zone by modulating the activity of Master neurons. If it licked at the precise time when the virtual cursor was located in the rewardable position, a small amount ($\sim 5 \mu\text{l}$) of water flowed immediately through the lick port, and the water droplet was swept away by the ongoing licking action.

We monitored the weight loss that resulted from the water restriction schedule. We ensured that through the whole training, the weight did not drop below 80% of its initial value, a consensus weight threshold in this model (58). To do so, mice were checked daily for weight and extra water/food intake was provided as needed to stabilize the weight. After these first sessions, we transitioned immediately to training the mice in the brain-machine interface task (1 session per day, 30 min), with one of the photostimulation feedback protocols, and only one feedback position rewarded.

The mice were trained with the same feedback protocol during five consecutive training sessions. There were no days off during these 5 days, except in the rare case of an unexpected technical problem. After the five training sessions, and if sufficient M1 activity was still present, we performed a new selection of Master neurons from scratch, and we restarted training the mouse with another feedback condition. There was generally a 2-day gap between different feedback protocols, except in three mice for which there was no pause in the training. We checked that previous learning did not bias the outcome of the following training (fig. S5B).

If the recording of one neuron was lost during the training, the active neighbor neuron with the largest spike shape was enrolled to replace it. If no additional neighbor neuron was available, the experiment kept going with a reduced count of Master neurons, down to a minimum of two Master neurons. We assessed the Master neuron population stability by counting cases where all Master units could not be reliably identified anymore at the start of one of the training sessions and had to be replaced with new units. This situation occurred once for two mice for the Bar feedback condition, two mice for the Full shuffle condition, and three mice for the No feedback condition. This amounts to 7 cases out of 152 transitions between sessions, thus about 5%. Note that in most of these cases, although we were unable to prove it, we suspected that a least one of the former Master neurons was picked as part of the new Master neuron pool.

Imaging of body movements

To probe whether there was a relationship between virtual cursor movements and mouse whisking, we acquired high-speed videography recordings of the animal including the contralateral whiskers, ear, and forepaw at 100 frames per second (camera; Baumer HXC-20; lens: 6 mm, F/1.4) and analyzed them using DeepLabCut-based marker-less tracking (64). Note that because of technical limitations, this was only done for a few sessions in the latest animals. First, we looked at the body movements during a session of spontaneous behavior. In these data, we failed to identify correlation of the body movements with the spiking activity of the Master neurons (fig. S10, A and B). Next, in three mice, we looked more specifically at the relationship between the virtual cursor movements and the whisker position during their first versus last training session in the Barrel shuffle condition. When doing so, we observed that the mice generally did not whisk and that instead their whiskerpad remained largely still. In addition, when they did perform whisker movements, we failed to identify a correlation with the optogenetic stimulation or the virtual cursor motor control. Consistent with previous brain-machine interface studies (65), there was, in particular, no sign of correlation in the fifth training session (for example, whisking bouts in one mouse in fig. S10C). Last, in the same three

mice, we analyzed one session of Bar playback, during which the animals received the Bar feedback spatiotemporal patterns without actively moving the virtual cursor. We tracked one of the right straddler whiskers (contralateral to the photostimulated S1 cortex) and the right ear. For both whisker and ear, we looked at the modulation of position following the axis where the movement amplitude was largest. In this dataset, we failed to identify any relationship between movements at the periphery and modulations of the virtual cursor that controls the Bar photostimulation (example in fig. S10D). Further looking into the relationship between frame photostimulation and peripheral movements, we also computed the average movement of the tracked whisker around the time of the entrance of the virtual cursor in the rewardable position. There, we also did not find any sign of a modulation of the whisker or ear (fig. S10E). Overall, these results suggest that performance in the Bar feedback condition is not solely due to S1 activation triggering specific body movements like whisking.

Offline spike sorting

Offline extraction of neuronal activity was performed using SpyKING CIRCUS (66). We confirmed that each online-sorted Master unit was properly spike-sorted by matching it with a specific offline-sorted unit through comparison of spike shapes and amplitudes across tetrodes. All additional, non-Master offline-sorted units were labeled as neighbor units.

Data analysis

All the data analysis was performed using the SciPy (version 1.10.0), NumPy (version 1.23.5), and matplotlib (version 3.7.0) packages in Python. We used nonparametric two-sided statistical tests, as indicated in the main text and/or figure legends. We applied Mann-Whitney tests for comparisons between distributions. We applied Wilcoxon paired tests when focusing explicitly on changes between two conditions for the same individuals (e.g., Fig. 6A). We used one Kruskal-Wallis H test to compare group medians (Fig. 7C). In addition, we have used an ANOVA for factor analysis (fig. S5B).

ICMS experiments

To confirm that the electrodes were located in the motor cortical area, we performed intracortical microstimulation (ICMS) at the end of the behavior sessions ($n = 3$ mice; fig. S2). We injected bipolar current pulses (amplitude 21 μ A/channel, duration 1.4 s, frequency 60 Hz, 50% duty cycle) through the 32-channel NeuroNexus silicon probe implanted in M1, in awake head-fixed animals. The contralateral whiskers were imaged using high-speed videography (camera: Baumer HXC-20; lens: 6 mm, F/1.4) at 300 frames per second for a duration of 9 s. A single trial consisted of 5 s before ICMS videography, followed by 1.4 s during ICMS stimulation and finally 2.6 s after ICMS. This procedure was repeated 14 times during a single session of ICMS experiment, with a 1-s inter-trial delay. In the ICMS videos, a central whisker was identified among all the whiskers in the field of view and tracked using the automated video tracking software DeepLabCut (64). The amplitude of ICMS-evoked whisker movement was defined as the mean whisker angle during the first 1 s of stimulation versus the 1 s immediately before. Latency of whisker movement was measured at the first frame with significant whisker movement amplitude (2 SDs above the mean).

Histology

After the experiment, mice were deeply anaesthetized with isoflurane (4 to 5%) and pentobarbital (150 mg/kg), then exsanguinated and perfused with 4% paraformaldehyde (PFA). The brains were extracted and stored overnight in 4% PFA. The brains were then transferred to a solution of phosphate-buffered saline for at least 24 hours. Fifty-micrometer slices were cut in the coronal plane and stained for cytochrome c oxidase. The location and depth of the silicon probe in the brain were traced by DiI depositing on the electrodes before their implantation and by localizing afterward the fluorescent dye present in the histological slices (fig. S2A).

Supplementary Materials

This PDF file includes:

Figs. S1 to S11

Table S1

REFERENCES AND NOTES

- R. S. Johansson, G. Westling, Roles of glabrous skin receptors and sensorimotor memory in automatic control of precision grip when lifting rougher or more slippery objects. *Exp. Brain Res.* **56**, 550–564 (1984).
- J. Monzée, Y. Lamarre, A. M. Smith, The effects of digital anesthesia on force control using a precision grip. *J. Neurophysiol.* **89**, 672–683 (2003).
- T. Brochier, M.-J. Boudreau, M. Paré, A. M. Smith, The effects of muscimol inactivation of small regions of motor and somatosensory cortex on independent finger movements and force control in the precision grip. *Exp. Brain Res.* **128**, 31–40 (1999).
- M. W. Mathis, A. Mathis, N. Uchida, Somatosensory cortex plays an essential role in forelimb motor adaptation in mice. *Neuron* **93**, 1493–1503.e6 (2017).
- A. T. Chesler, M. Szczot, D. Bharucha-Goebel, M. Čeko, S. Donkervoort, C. Laubacher, L. H. Hayes, K. Alter, C. Zampieri, C. Stanley, A. M. Innes, J. K. Mah, C. M. Grossmann, N. Bradley, D. Nguyen, A. R. Foley, C. E. Le Pichon, C. G. Bönnemann, The role of *PIEZO2* in human mechanosensation. *N. Engl. J. Med.* **375**, 1355–1364 (2016).
- R. C. Miall, N. M. Kitchen, S.-H. Nam, H. Lefumat, A. G. Renault, K. Ørstavik, J. D. Cole, F. R. Sarlegna, Proprioceptive loss and the perception, control and learning of arm movements in humans: Evidence from sensory neuronopathy. *Exp. Brain Res.* **236**, 2137–2155 (2018).
- R. L. Sainburg, M. F. Ghilardi, H. Poizner, C. Ghez, Control of limb dynamics in normal subjects and patients without proprioception. *J. Neurophysiol.* **73**, 820–835 (1995).
- S. N. Flesher, J. E. Downey, J. M. Weiss, C. L. Hughes, A. J. Herrera, E. C. Tyler-Kabara, M. L. Boninger, J. L. Collinger, R. A. Gaunt, A brain-computer interface that evokes tactile sensations improves robotic arm control. *Science* **372**, 831–836 (2021).
- J. E. O'Doherty, S. Shokur, L. E. Medina, M. A. Lebedev, M. A. L. Nicolelis, Creating a neuroprosthesis for active tactile exploration of textures. *Proc. Natl. Acad. Sci. U.S.A.* **116**, 21821–21827 (2019).
- M. Armenta Salas, L. Bashford, S. Kellis, M. Jafari, H. Jo, D. Kramer, K. Shanfield, K. Pejisa, B. Lee, C. Y. Liu, R. A. Andersen, Proprioceptive and cutaneous sensations in humans elicited by intracortical microstimulation. *eLife* **7**, e32904 (2018).
- D. H. O'Connor, S. A. Hires, Z. V. Guo, N. Li, J. Yu, Q.-Q. Sun, D. Huber, K. Svoboda, Neural coding during active somatosensation revealed using illusory touch. *Nat. Neurosci.* **16**, 958–965 (2013).
- J. E. O'Doherty, M. A. Lebedev, P. J. Ifft, K. Z. Zhuang, S. Shokur, H. Bleuler, M. A. L. Nicolelis, Active tactile exploration using a brain-machine-brain interface. *Nature* **479**, 228–231 (2011).
- R. Romo, A. Hernández, A. Zainos, E. Salinas, Somatosensory discrimination based on cortical microstimulation. *Nature* **392**, 387–390 (1998).
- G. A. Tabot, J. F. Dammann, J. A. Berg, F. V. Tenore, J. L. Boback, R. J. Vogelstein, S. J. Bensmaia, Restoring the sense of touch with a prosthetic hand through a brain interface. *Proc. Natl. Acad. Sci. U.S.A.* **110**, 18279–18284 (2013).
- A. Abbasi, D. Goueytes, D. E. Shulz, V. Ego-Stengel, L. Estebanez, A fast intracortical brain-machine interface with patterned optogenetic feedback. *J. Neural Eng.* **15**, 046011 (2018).
- M. Prsa, G. L. Galiñanes, D. Huber, Rapid integration of artificial sensory feedback during operant conditioning of motor cortex neurons. *Neuron* **93**, 929–939.e6 (2017).
- S. Badde, T. Heed, Towards explaining spatial touch perception: Weighted integration of multiple location codes. *Cogn. Neuropsychol.* **33**, 26–47 (2016).
- S. N. Flesher, J. L. Collinger, S. T. Foldes, J. M. Weiss, J. E. Downey, E. C. Tyler-Kabara, S. J. Bensmaia, A. B. Schwartz, M. L. Boninger, R. A. Gaunt, Intracortical microstimulation of human somatosensory cortex. *Sci. Transl. Med.* **8**, 361ra141 (2016).
- K. Hartmann, E. E. Thomson, I. Zea, R. Yun, P. Mullen, J. Canarick, A. Huh, M. A. L. Nicolelis, Embedding a panoramic representation of infrared light in the adult rat somatosensory cortex through a sensory neuroprosthesis. *J. Neurosci.* **36**, 2406–2424 (2016).
- W. Penfield, E. Boldrey, Somatic motor and sensory representation in the cerebral cortex of man as studied by electrical stimulation. *Brain* **60**, 389–443 (1937).
- M. E. Diamond, E. Arabzadeh, Whisker sensory system—From receptor to decision. *Prog. Neurobiol.* **103**, 28–40 (2013).
- C. C. H. Petersen, Sensorimotor processing in the rodent barrel cortex. *Nat. Rev. Neurosci.* **20**, 533–546 (2019).
- M. Deschenes, Vibrissal afferents from trigeminus to cortices. *Scholarpedia* **4**, 7454 (2009).
- D. Feldmeyer, Excitatory neuronal connectivity in the barrel cortex. *Front. Neuroanat.* **6**, 24 (2012).
- L. Estebanez, I. Férézou, V. Ego-Stengel, D. E. Shulz, Representation of tactile scenes in the rodent barrel cortex. *Neuroscience* **368**, 81–94 (2018).
- V. Jacob, J. Le Cam, V. Ego-Stengel, D. E. Shulz, Emergent properties of tactile scenes selectively activate barrel cortex neurons. *Neuron* **60**, 1112–1125 (2008).
- M. E. Vilarchao, L. Estebanez, D. E. Shulz, I. Férézou, Supra-barrel distribution of directional tuning for global motion in the mouse somatosensory cortex. *Cell Rep.* **22**, 3534–3547 (2018).
- K. J. Laboy-Juárez, T. Langberg, S. Ahn, D. E. Feldman, Elementary motion sequence detectors in whisker somatosensory cortex. *Nat. Neurosci.* **22**, 1438–1449 (2019).
- P.-J. Arduin, Y. Fregnac, D. E. Shulz, V. Ego-Stengel, “Master” neurons induced by operant conditioning in rat motor cortex during a brain-machine interface task. *J. Neurosci.* **33**, 8308–8320 (2013).
- L. Madisen, T. Mao, H. Koch, J. Zhuo, A. Berenyi, S. Fujisawa, Y.-W. A. Hsu, A. J. Garcia, X. Gu, S. Zanella, J. Kidney, H. Gu, Y. Mao, B. M. Hooks, E. S. Boyden, G. Buzsáki, J. M. Ramirez, A. R. Jones, K. Svoboda, X. Han, E. E. Turner, H. Zeng, A toolbox of Cre-dependent optogenetic transgenic mice for light-induced activation and silencing. *Nat. Neurosci.* **15**, 793–802 (2012).
- S. H. Scott, A functional taxonomy of bottom-up sensory feedback processing for motor actions. *Trends Neurosci.* **39**, 512–526 (2016).
- T. C. Marzullo, C. R. Miller, D. R. Kipke, Suitability of the cingulate cortex for neural control. *IEEE Trans. Neural Syst. Rehabil. Eng.* **14**, 401–409 (2006).
- Y. Sakurai, S. Takahashi, Conditioned enhancement of firing rates and synchrony of hippocampal neurons and firing rates of motor cortical neurons in rats. *Eur. J. Neurosci.* **37**, 623–639 (2013).
- R. S. Johansson, J. R. Flanagan, Coding and use of tactile signals from the fingertips in object manipulation tasks. *Nat. Rev. Neurosci.* **10**, 345–359 (2009).
- H. Lassagne, D. Goueytes, D. E. Shulz, L. Estebanez, V. Ego-Stengel, Continuity within the somatosensory cortical map facilitates learning. *Cell Rep.* **39**, 110617 (2022).
- J. H. Kaas, Topographic maps are fundamental to sensory processing. *Brain Res. Bull.* **44**, 107–112 (1997).
- M. L. Andermann, C. I. Moore, A somatotopic map of vibrissa motion direction within a barrel column. *Nat. Neurosci.* **9**, 543–551 (2006).
- L. Estebanez, J. Bertherat, D. E. Shulz, L. Bourdieu, J.-F. Léger, A radial map of multi-whisker correlation selectivity in the rat barrel cortex. *Brain Commun.* **7**, 13528 (2016).
- Y. Kremer, J.-F. Leger, D. Goodman, R. Brette, L. Bourdieu, Late emergence of the vibrissa direction selectivity map in the rat barrel cortex. *J. Neurosci.* **31**, 10689–10700 (2011).
- D. J. Simons, Response properties of vibrissa units in rat SI somatosensory neocortex. *J. Neurophysiol.* **41**, 798–820 (1978).
- L. Estebanez, S. E. Boustani, A. Destexhe, D. E. Shulz, Correlated input reveals coexisting coding schemes in a sensory cortex. *Nat. Neurosci.* **15**, 1691–1699 (2012).
- I. Ferezou, S. Bolea, C. C. H. Petersen, Visualizing the cortical representation of whisker touch: Voltage-sensitive dye imaging in freely moving mice. *Neuron* **50**, 617–629 (2006).
- M. Fu, Y. Zuo, Experience-dependent structural plasticity in the cortex. *Trends Neurosci.* **34**, 177–187 (2011).
- M. C. Dadarlat, J. E. O'Doherty, P. N. Sabes, A learning-based approach to artificial sensory feedback leads to optimal integration. *Nat. Neurosci.* **18**, 138–144 (2015).
- R. Pancholi, A. Sun-Yan, S. Peron, Microstimulation of sensory cortex engages natural sensory representations. *Curr. Biol.* **33**, 1765–1777.e5 (2023).
- B. Akitake, H. M. Douglas, P. K. LaFosse, M. Beiran, C. E. Deveau, J. O'Rawe, A. J. Li, L. N. Ryan, S. P. Duffy, Z. Zhou, Y. Deng, K. Rajan, M. H. Histed, Amplified cortical neural responses as animals learn to use novel activity patterns. *Curr. Biol.* **33**, 2163–2174.e4 (2023).
- A. C. Koralek, X. Jin, J. D. Long II, R. M. Costa, J. M. Carmena, Corticostriatal plasticity is necessary for learning intentional neuroprosthetic skills. *Nature* **483**, 331–335 (2012).

48. J. A. Hobbs, R. B. Towal, M. J. Z. Hartmann, Spatiotemporal patterns of contact across the rat vibrissal array during exploratory behavior. *Front. Behav. Neurosci.* **9**, 356 (2016).
49. E. E. Fetz, Operant conditioning of cortical unit activity. *Science* **163**, 955–958 (1969).
50. C. T. Moritz, S. I. Perlmutter, E. E. Fetz, Direct control of paralysed muscles by cortical neurons. *Nature* **456**, 639–642 (2008).
51. P. T. Sadtler, K. M. Quick, M. D. Golub, S. M. Chase, S. I. Ryu, E. C. Tyler-Kabara, B. M. Yu, A. P. Batista, Neural constraints on learning. *Nature* **512**, 423–426 (2014).
52. V. R. Athalye, K. Ganguly, R. M. Costa, J. M. Carmena, Emergence of coordinated neural dynamics underlies neuroprosthetic learning and skillful control. *Neuron* **93**, 955–970.e5 (2017).
53. E. R. Oby, M. D. Golub, J. A. Hennig, A. D. Degenhart, E. C. Tyler-Kabara, B. M. Yu, S. M. Chase, A. P. Batista, New neural activity patterns emerge with long-term learning. *Proc. Natl. Acad. Sci. U.S.A.* **116**, 15210–15215 (2019).
54. A. E. Papale, B. M. Hooks, Circuit changes in motor cortex during motor skill learning. *Neuroscience* **368**, 283–297 (2018).
55. G. Valle, A. Mazzoni, F. Iberite, E. D'Anna, I. Strauss, G. Granata, M. Controzzi, F. Clemente, G. Rognini, C. Cipriani, T. Stieglitz, F. M. Petrini, P. M. Rossini, S. Micera, Biomimetic intraneural sensory feedback enhances sensation naturalness, tactile sensitivity, and manual dexterity in a bidirectional prosthesis. *Neuron* **100**, 37–45.e7 (2018).
56. S. J. Bensmaia, L. E. Miller, Restoring sensorimotor function through intracortical interfaces: Progress and looming challenges. *Nat. Rev. Neurosci.* **15**, 313–325 (2014).
57. A. Holtmaat, T. Bonhoeffer, D. K. Chow, J. Chuckowree, V. De Paola, S. B. Hofer, M. Hübener, T. Keck, G. Knott, W.-C. A. Lee, R. Mostany, T. D. Mrsic-Flogel, E. Nedivi, C. Portera-Cailliau, K. Svoboda, J. T. Trachtenberg, L. Wilbrecht, Long-term, high-resolution imaging in the mouse neocortex through a chronic cranial window. *Nat. Protoc.* **4**, 1128–1144 (2009).
58. Z. V. Guo, S. A. Hires, N. Li, D. H. O'Connor, T. Komiyama, E. Ophir, D. Huber, C. Bonardi, K. Morandell, D. Gutnisky, S. Peron, N. Xu, J. Cox, K. Svoboda, Procedures for behavioral experiments in head-fixed mice. *PLOS ONE* **9**, e88678 (2014).
59. M. Okun, A. Lak, M. Carandini, K. D. Harris, Long term recordings with immobile silicon probes in the mouse cortex. *PLOS ONE* **11**, e0151180 (2016).
60. S. Ceballo, Z. Piwkowska, J. Bourg, A. Daret, B. Bathellier, Targeted cortical manipulation of auditory perception. *Neuron* **104**, 1168–1179.e5 (2019).
61. G. Nagel, T. Szellas, W. Huhn, S. Kateriya, N. Adeishvili, P. Berthold, D. Ollig, P. Hegemann, E. Bamberg, Channelrhodopsin-2, a directly light-gated cation-selective membrane channel. *Proc. Natl. Acad. Sci. U.S.A.* **100**, 13940–13945 (2003).
62. P. M. Knutsen, C. Mateo, D. Kleinfeld, Precision mapping of the vibrissa representation within murine primary somatosensory cortex. *Philos. Trans. R. Soc. B* **371**, 20150351 (2016).
63. P. J. Drew, D. E. Feldman, Intrinsic signal imaging of deprivation-induced contraction of whisker representations in rat somatosensory cortex. *Cereb. Cortex* **19**, 331–348 (2009).
64. A. Mathis, P. Mamidanna, K. M. Cury, T. Abe, V. N. Murthy, M. W. Mathis, M. Bethge, DeepLabCut: Markerless pose estimation of user-defined body parts with deep learning. *Nat. Neurosci.* **21**, 1281–1289 (2018).
65. J. K. Chapin, K. A. Moxon, R. S. Markowitz, M. A. L. Nicolelis, Real-time control of a robot arm using simultaneously recorded neurons in the motor cortex. *Nat. Neurosci.* **2**, 664–670 (1999).
66. P. Yger, G. L. Spampinato, E. Esposito, B. Lefebvre, S. Deny, C. Gardella, M. Stimberg, F. Jetter, G. Zeck, S. Picaud, J. Duebel, O. Marre, A spike sorting toolbox for up to thousands of electrodes validated with ground truth recordings in vitro and in vivo. *eLife* **7**, e34518 (2018).

Acknowledgments: We thank I. Férézou for advice on experimental design and analysis; A. Tolboom for analysis support; and E. Ahissar, B. Barbour, K. Benchenane, S. B. Hamed, S. Bensmaia, D. Feldman, E. Harrell, and G. Sumbre for comments on an earlier version of the manuscript. A. Daret and G. Hucher provided experimental support. **Funding:** This work was supported by FRM (Equipe FRM DEQ20170336761), CNRS (80|Prime), ANR Neurowhisk, ANR MesoBrain, ANR MotorSense, Lidex NeuroSaclay, Idex Brainscopes, iCODE, FRC (AAP 2018), and Fondation 3DS. **Author contributions:** Funding: D.E.S. and V.E.-S. Methodology: D.E.S., L.E., and V.E.-S. Supervision: D.E.S., L.E., and V.E.-S. Experiments: A.A. and H.L., with support from L.E. and D.G. Data analysis: L.E. and A.A., with support from H.L. Writing: L.E., V.E.-S., and D.E.S., with input from all authors. **Competing interests:** The authors declare that they have no competing interests. **Data and materials availability:** All data needed to evaluate the conclusions in the paper are present in the paper and/or the Supplementary Materials. Individual data values are available at the following DOI: 10.5281/zenodo.7958465.

Submitted 12 February 2023

Accepted 23 August 2023

Published 22 September 2023

10.1126/sciadv.adh1328